CHEMCATCHEM

DOI: 10.1002/cctc.201100179

Synthesis of CeO_2-Based Quantum Dots through a Polyol-Hydrolysis Method for Fuel-Borne Catalysts

Ying Xin,[a] Xi Yang,[a] Pin Jiang,[a] Zhaoliang Zhang,*[a] Zhongpeng Wang,[a] and Yihe Zhang*[a, b]

The transparent colloidal solutions of monodisperse CeO_2-based quantum dots (QDs) were prepared by heating a triethylene glycol (TEG) solution of $Ce(NO_3)_3{\cdot}6H_2O$ (and $Fe(NO_3)_3{\cdot}9H_2O$) at 180 °C. The CeO_2-based QDs were characterized by X-ray powder diffraction (XRD), dynamic light scattering (DLS), transmission electron microscopy (TEM), UV/vis absorption spectra and Brunauer–Emmett–Teller (BET) surface area. CeO_2-based QDs with uniform particle size below 5 nm exhibit narrow size distribution, quantum effect, good re-dispersion ability and high surface area. For the formation of these QDs, a polyol-hydrolysis mechanism is proposed. CeO_2 QDs are applied in fuel borne catalysts (FBCs) for diesel soot combustion, which exhibit excellent activity at a rather low temperature, owing to the homogeneous and large number of contact points between the catalyst and the soot. The doping with Fe can further improve the selectivity to CO_2.

Introduction

Soot particulate matter (PM) emissions from diesel engines cause severe environmental and health problems, which require that they be controlled. The diesel particulate filter (DPF) is the most promising technology for the removal of soot.[1–6] However, the collected particles must be removed by oxidation to prevent excessive pressure drop in the exhaust system, which would otherwise adversely affect engine operation. Therefore, the ability to regenerate the DPF on which particulates are deposited is considered one of the major issues in diesel engine applications of DPF systems. Unfortunately, the ignition temperature of soot (>450 °C) is beyond the normal diesel exhaust temperature range (150–400 °C). As a catalytic means of deliberately lowering the ignition temperature of soot into the typical range of diesel engine exhaust temperatures, adding a fuel borne catalyst (FBC) to the fuel can rapidly and completely regenerate a DPF. This is because the combustion of the resulting fuel leads to in-cylinder generation of catalyst particles intimately mixed with the soot which is simultaneously formed from incomplete combustion of the fuel.[7]

Among various FBCs, CeO_2-based oxides attract special attention, owing to their oxygen storage capacity (OSC).[7–9] The oxides are commonly doped with Fe, the introduction of which [Fe/(Ce+Fe) = 5–20 wt.%] can greatly improve the kinetic performance of soot combustion.[10,11] To ensure the intimate contact with the diesel PM on DPF, the FBCs with the smallest size are highly desirable. Furthermore, FBCs should also be compatible, dispersible and stable in organic solvents. There are many methods to prepare the CeO_2-based oxides with diameters below 10 nm, such as homogeneous precipitation,[12,13] combustion,[14] hydrothermal,[15,16] surfactant-assisted,[17] polymer complex,[18] microemulsion,[19,20] solvothermal,[21] and polyol mediated methods.[22] However, the monodispersed ceria nanoparticles with diameters below 5 nm are more difficult and inconvenient to prepare, because they have a stronger tendency to agglomerate.

The polyol method has been widely used for the preparation of single and mixed metal oxide nanoparticles,[15,23–27] in which the polyols are claimed to prevent aggregation and act as solvent, stabilizer, and reducing agent. For instance, Inoue et al.[15] reported that the reaction of Ce metal in 2-methoxyethanol at 200–250 °C yields a transparent colloidal solution of ultrafine (2 nm size) CeO_2 particles. Cai et al.[23] prepared monodisperse Fe_3O_4 nanoparticles with the high-temperature solution reduction of $[Fe(acac)_3]$ by a series of polyols and found that only the reaction of $[Fe(acac)_3]$ in triethylene glycol (TEG) resulted in non-aggregated nanoparticles. Feldmann and coworkers[24–27] obtained concentrated, colloidally stable solutions of Fe_2O_3 and CeO_2 by heating the properly dissolved metal precursor materials (e.g. acetate, oxalate, alcoholate, halogenide) in diethylene glycol (DEG) with defined amount of water. However, the minimum particle diameter is 30 nm.

Herein, we extend the research cited above and develop a simple and low-cost polyol-hydrolysis method to directly produce non-aggregated CeO_2-based nanoparticles with diameters below 5 nm, which are in the size range of quantum dots

[a] Y. Xin, X. Yang, P. Jiang, Prof. Z. Zhang, Prof. Z. Wang, Prof. Y. Zhang
Shandong Provincial Key Laboratory of Fluorine Chemistry
and Chemical Materials, School of Chemistry and Chemical Engineering,
University of Jinan, 106 Jiwei Road, Jinan 250022 (China)
Fax: (+86) 531-8973-6032
E-mail: chm_zhangzl@ujn.edu.cn

[b] Prof. Y. Zhang
National Laboratory of Mineral Materials
China University of Geosciences (Beijing)
29 Xueyuan Road, Beijing 100083 (China)
E-mail: zyh@cugb.edu.cn

Supporting information for this article is available on the WWW under http://dx.doi.org/10.1002/cctc.201100179.

(QDs). The structure and properties of the CeO_2-based QDs were studied and confirmed by X-ray powder diffraction (XRD), high resolution transmission electron microscopy (HRTEM) equipped with energy dispersive spectroscopy (EDS), selective area electron diffraction (SAED), dynamic light scattering (DLS), UV/vis spectroscopy, field emission scanning electron microscopy (FESEM) equipped with EDS, Fourier transform infrared (FTIR) spectroscopy, nuclear magnetic resonance (NMR) spectroscopy and Brunauer-Emmett-Teller (BET) surface area. These studies reveal that CeO_2-based QDs exhibit narrow size distribution, quantum effect, good re-dispersion ability and high BET surface area, which are expected to be applicable in various fields. As FBCs, CeO_2-based QDs show improved activity for soot combustion compared with their larger nanometer counterparts

Results and Discussion

The products synthesized with TEG, ethylene glycol (EG), DEG, and polyethylene glycol (a molecular weight of ≈400, hereafter referred to as PEG) were named Ce-TEG, Ce-EG, Ce-DEG and Ce-PEG, respectively. Ce-TEG-H_2O represents the addition of 2 mL water during synthesis. The CeO_2 doped with Fe (molar ratio: Ce/Fe = 9/1) was named Ce–Fe-TEG. The solid samples were obtained by washing and drying processes.

CeO_2 Quantum dots

In polar solvent, the CeO_2 QDs synthesized using TEG form a yellow transparent solution. When the solution is kept in a closed bottle, it is stable for at least several months. As shown in the XRD pattern in Figure 1, all the peaks can be indexed to

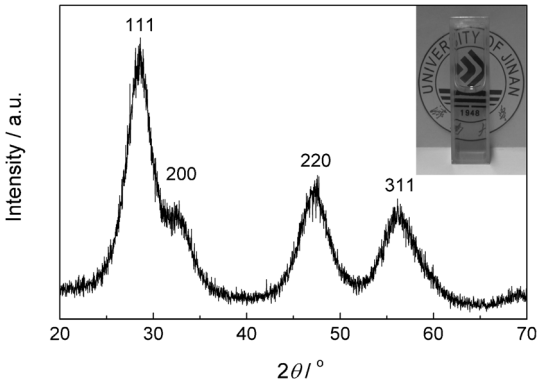

Figure 1. XRD pattern of Ce-TEG solid sample; inset: photograph of Ce-TEG.

a pure cubic fluorite phase CeO_2 (*Fm*3*m*, JCPDS 34–0394). The peak broadening of XRD patterns reveals the significantly small size of the resulting crystallites. The average crystallite size calculated using Scherrer's formula is 2.9 nm. The representative TEM images (Figure 2a and b) show that the colloidal solution contains non-agglomerated primary particles with an average particle size of 2.4 nm (Figure 2c). DLS measurement

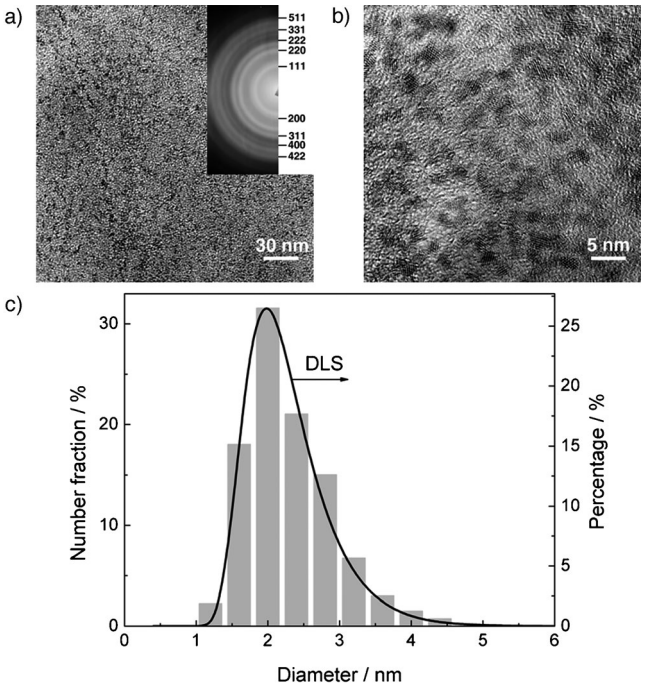

Figure 2. a) TEM image and SAED pattern (inset) of Ce-TEG; b) HRTEM image of Ce-TEG; c) Histogram of particle size distribution and DLS spectrum .

(Figure 2c) reveals a narrow distribution with a mean size of 2.3 nm. Furthermore, the HRTEM image (Figure 2b) shows that each particle is a single crystal and the preferred plane on the surface is (111). The reticular distances indexed from the SAED pattern (Figure 2a, inset) exactly match those expected from CeO_2.

The room temperature UV/vis absorption spectra of Ce-TEG (Figure 3) show a strong absorption band in the UV region, whereas no absorption was detected above $\lambda = 400$ nm. The

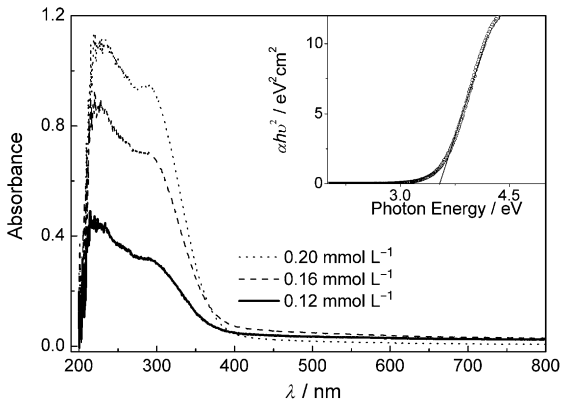

Figure 3. UV/vis absorption spectra of three different concentrations of Ce-TEG; inset: normalized plot of $(\alpha h\nu)^2$ versus Ephoton for Ce-TEG.

absorbance measurements conform to the Lambert–Beer law, suggesting that the ultrafine ceria particles are well dispersed with no evidence of agglomeration under the concentrations necessary for UV measurement. The plot of $(\alpha h\nu)^2$ versus

photon energy for the sample is shown in the inset of Figure 3. It reveals that the band gap of CeO_2 QDs is about 3.54 eV, which is larger than that of the bulk CeO_2 (E_g = 3.19 eV[19]). This blue-shifting phenomenon results from the reduction of particle size due to quantum confinement effect.

Re-dispersion ability

The CeO_2 QDs can be easily re-dispersed in an aqueous solution, ethanol, and other polar solvents by ultrasonication. Upon re-dispersion by ultrasonication, a clear Tyndall effect was observed for CeO_2 QDs in TEG, water, and ethanol under laser irradiation (Figure S1), which normally occurs in a well-dispersed colloidal system. This is attributed to the formation of a steric barrier from the strong hydrophilic organic ligands coated on the QDs, which prevent the growth and agglomeration of QDs.[25]

The species coated on the surface of the QDs were first checked by FTIR. A strong Ce–O absorption band at $\tilde{\nu} \approx 500\ cm^{-1}$ (Figure 4b) is evidence of the formation of

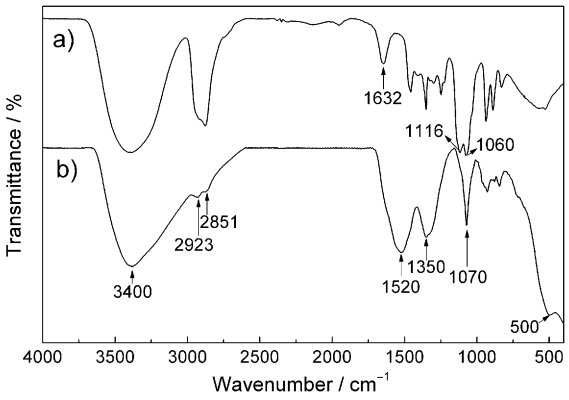

Figure 4. FTIR spectrum of a) pure TEG and b) Ce-TEG solid product.

CeO_2.[18,28,29] The broad band at $\tilde{\nu} = 3400\ cm^{-1}$ is related to O-H stretching vibration arising from surface hydroxyl groups. Two bands at $\tilde{\nu} = 2923$ and $2851\ cm^{-1}$ are assigned to the C–H stretching vibration, while the strong band at $\tilde{\nu} = 1350\ cm^{-1}$ is distributed to C–H deformation vibration. Moreover, the bands at $\tilde{\nu} = 1116$–$1050\ cm^{-1}$ are ascribed to C–O stretching vibration.[23] The band at $\tilde{\nu} = 1520\ cm^{-1}$ corresponds to water.[28] These assignments support the successful coating of TEG on the surface of CeO_2 QDs, which was further confirmed by ^{1}H NMR spectroscopy. As shown in Figure S2, the values of the proton resonances for the Ce-TEG solid product are the same as those of pure TEG. The presence of the signals due to the main chain protons of TEG, $\delta = 1.0$–1.1 ppm (-CH_2-CH_2-) and 3.4–3.7 ppm (-O-CH_2-CH_2-O-), were also observed.

Effects of the type of polyol

The effects of using different types of polyols and the addition of water were investigated. The representative photographs and TEM images of the samples are shown in Figure 5. In the

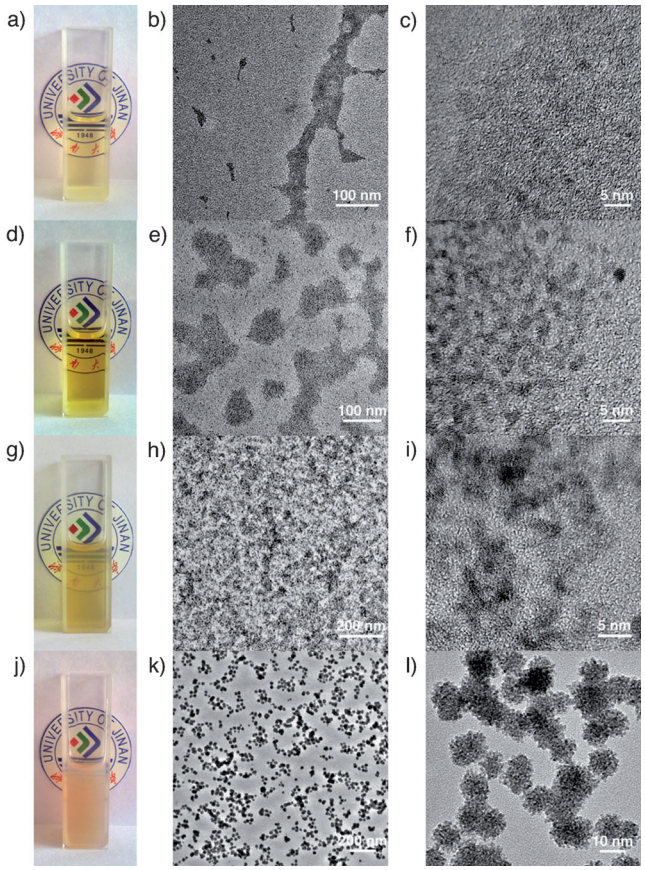

Figure 5. The photographs and TEM images of the samples. a), b), and c) Ce-EG; d), e), and f) Ce-DEG; g), h), and i) Ce-PEG; j), k), and l) Ce-TEG-H_2O.

case of Ce-EG, a light yellow transparent solution was obtained (Figure 5a), which suggests a low yield of the product. Figure 5b and c show that the CeO_2 particles are considerably aggregated and not well crystallized (reaction at 150 °C owing to the 197 °C boiling point of EG, see Experimental section). As to Ce-DEG, although the color of Ce-DEG (Figure 5d) is similar to that of Ce-TEG, the dispersion of the CeO_2 particles is not uniform (Figure 5e). Unlike the first two samples, suspensions were obtained for both Ce-PEG (Figure 5g) and Ce-TEG-H_2O (Figure 5j). Furthermore, Ce-TEG-H_2O is composed of $Ce(OH)_3$ rather than CeO_2 based on the color of the product. These facts suggest that the ether group plays an important role in the yield, while the length of the polyol chain determines the dispersion of the product. The adoption of PEG and addition of excess water result in a suspension which was not expected.

Formation mechanism

The TG/DTA/DTG patterns of $Ce(NO_3)_3 \cdot 6H_2O$ (Figure S3) show two thermal steps at 203 °C and 261 °C, which can be ascribed to the desorption of crystalline water and the decomposition of the nitrate to the corresponding oxide, respectively. We deduced that the reflux of the TEG solution of $Ce(NO_3)_3 \cdot 6H_2O$ at 180 °C results in neither the loss of crystalline water nor the decomposition of the nitrate. Furthermore, the evolution of NO_x

gas was not observed during the heating process. Therefore, the reduction mechanism of TEG that is well-known for the polyol method might be excluded. Moreover, because of the absence of a strong base, the precipitation mechanism is also impossible.

The hydrolysis mechanism has been reported for synthesis of ZnO,[30] Fe_3O_4,[31] and In_2O_3[32] nanocrystals. Inspired by this mechanism and the above experimental results, we explain the formation process of CeO_2-TEG as follows (Scheme 1): First,

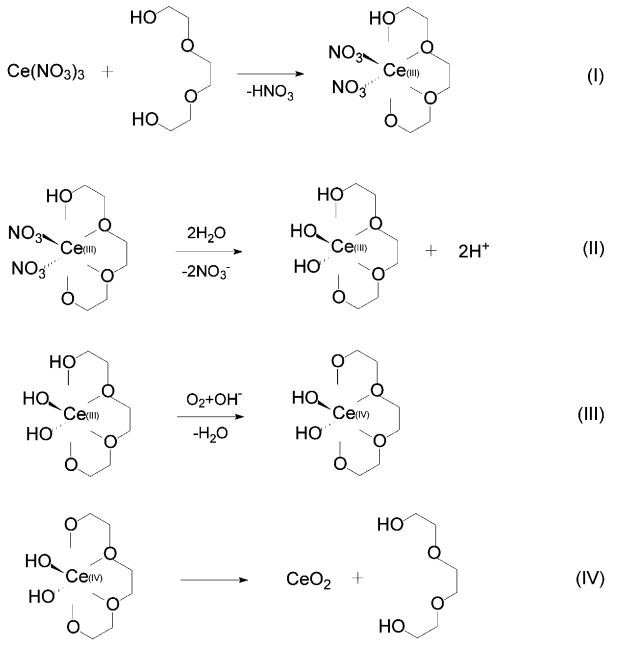

Scheme 1. Proposed mechanism for Ce chelated complex formation (I), hydrolysis of complexes (II), oxidation and dehydration of hydrolysates (III), and decomposition of complexes (IV).

the chelating Ce^{III} alkoxide complexes are formed via the chelation of Ce^{3+} by the ether groups and the terminal hydroxyl groups in polyols (reaction I). Secondly, the hydrolysis of Ce^{III} alkoxide complexes occurs (Reaction II). Thirdly, the Ce^{III} alkoxide complexes are oxidized and dehydrated by dissolved oxygen to form the Ce^{IV} alkoxide complexes (Reaction III). Finally, the decomposition of Ce^{IV} alkoxide complexes yields CeO_2 (Reaction IV).

Unlike strongly basic solvents (such as ammonia) that rapidly react with Ce^{3+} in an uncontrollable manner or neutral solvents (such as water) that result in the unhydrolysis of Ce^{3+}, the ether groups and the terminal hydroxyl groups of polyols provide a special basic condition for the hydrolysis of Ce^{3+} in a controllable manner.[12] As a strong Lewis base, the ether oxygen is prone to be an acceptor of the protons produced in Reactions I and II (Scheme 1) to form diethyloxonium ions.[33,34] Owing to the absence of the ether group in EG, Ce^{3+} ions can only chelate with the terminal hydroxyl groups and the hydrolysis proceeds poorly, resulting in the low yield with EG. However, with the increasing number of ether groups in the polyols (Ce-DEG, Ce-TEG and Ce-PEG), Ce^{3+} ions are coordinated not only to the terminal hydroxyl groups, but also to the ether groups. Thus, the hydrolysis proceeds smoothly and the yield is improved. When H_2O (2 mL) was added, the oxidation and dehydration process of Ce^{III} hydrates was suppressed (Reaction III). As expected from Reaction II, the $Ce(OH)_3$ was produced (Figure 5j), while, simultaneously, the protective layer on the $Ce(OH)_3$ might have been destroyed. The flower-like agglomerates composed of smaller nanoparticles (Figure 5l) occur through random aggregation that minimizes surface energy.

Synthesis of the Ce–Fe complex oxide quantum dots

The strategy can be extended to prepare Ce and Fe complex oxide QDs (Ce–Fe-TEG). The composition of the as formed yellow-brown transparent solution (Figure 6a) determined by

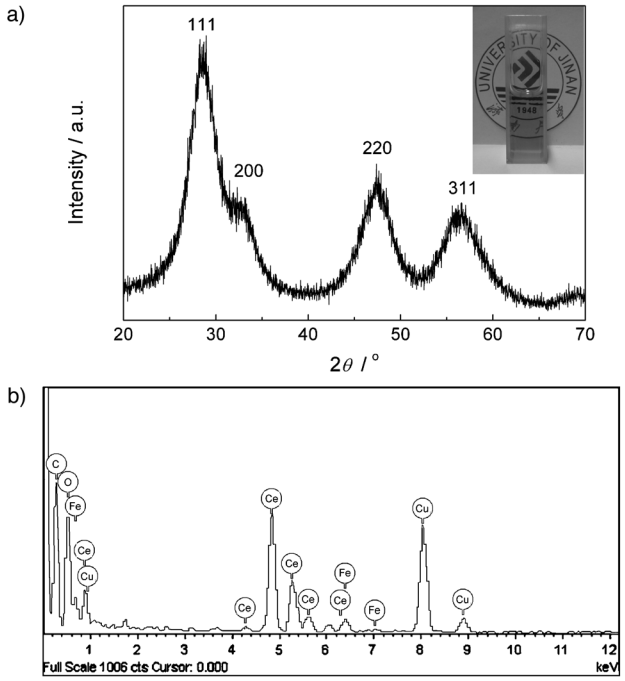

Figure 6. a) XRD pattern, the photograph (inset) and b) the EDS spectrum of the Ce–Fe complex oxide QDs.

the EDS analysis (Figure 6b), is nearly the same as the nominal value (The molar ratio of Ce/Fe equals to 0.91/0.09, namely $Ce_{0.91}Fe_{0.09}O_2$). Furthermore, FESEM and the corresponding distribution mapping were used to investigate the dispersion of Ce, Fe and O elements (Figure 7). Analysis of Figure 7 reveals that Ce and Fe elements are well dispersed. However, TEM images (Figure 8) show weak agglomerates with individual particle sizes of $\approx$3.1 nm. The SAED pattern (Figure 8a, inset) was indexed to that from the Ce–Fe oxide solid solution. A clear Tyndall effect can also be observed for $Ce_{0.91}Fe_{0.09}O_2$ QDs in TEG, water and ethanol under laser irradiation (Figure S4). Analysis of the FTIR spectrum (Figure S5) reveals the attachment of TEG on the surfaces of the $Ce_{0.91}Fe_{0.09}O_2$ QDs.

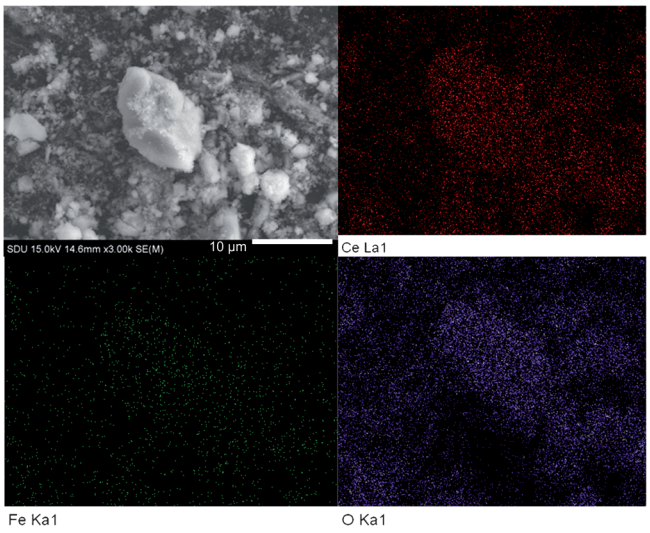

Figure 7. FESEM image and the corresponding distribution map of Ce, Fe, and O elements for the Ce–Fe complex oxide QDs.

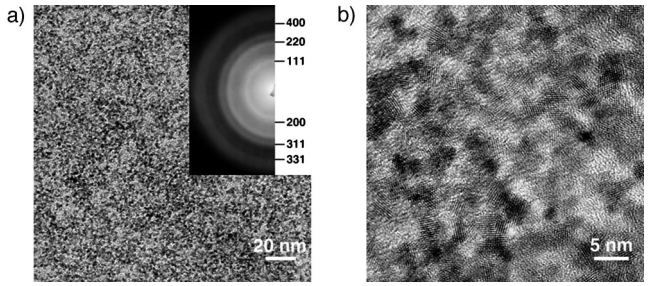

Figure 8. a) TEM image and SAED pattern (inset); b) HRTEM image of Ce–Fe-TEG.

Catalytic activity

As shown in Figure 9a and b, the temperature-programmed oxidation (TPO) curves of QDs and soot mixture, which have a main peak and a shoulder. As discussed above, the shoulder can be ascribed to the oxidation of TEG coated on the QD surface. According to our previous work,[11] the mixture of QDs and soot is diluted with silica to aid heat transfer. Therefore, the soot combustion was not affected by the oxidation of the remaining TEG on QDs. The main peak temperature (T_{max}) represents the intrinsic activity of QDs.

A multivariate non-linear regression model is used to deconvolute the overlapping processes.[35] The TPO result demonstrated that the $T_{max} = \approx 350\,^{\circ}C$ for CeO_2 QDs$\approx$, which is 45 °C lower than that of the nanometer CeO_2 counterpart ($\approx$14.5 nm).[11] $Ce_{0.91}Fe_{0.09}O_2$ has nearly identical activity to CeO_2 (Figure 9b); however, the selectivity for CO_2 is 100%. Because the BET surface areas were 245 and 303 m^2g^{-1} for CeO_2 and $Ce_{0.91}Fe_{0.09}O_2$, respectively, the high activity for soot combustion is attributed to the high surface area and especially small particle size of QDs, which results in a large number of contact points between the catalyst and the soot. This is confirmed by TEM. As shown in Figure 9c, the amorphous soot was surrounded by CeO_2 QDs, which ameliorates contact conditions.

Conclusions

CeO_2 and $Ce_{0.91}Fe_{0.09}O_2$ quantum dots were successfully synthesized via a simple and low-cost polyol route, which is based on the hydrolysis of metal alkoxide complexes at elevated temperatures in triethylene glycol. The stable colloidal solutions of QDs show a uniform particle size below 5 nm, good re-dispersion ability and high specific surface area. CeO_2 QD FBCs exhibit excellent activity at relatively low temperatures for soot combustion. The doping with Fe can further improve the selectivity to CO_2.

Experimental Section

Synthesis of CeO_2-based quantum dots

All chemicals used in our experiments were of analytical reagent (AR) grade and purchased from Sinopharm Chemical Reagent Co., Ltd., China. In a typical synthesis, 2 mmol of $Ce(NO_3)_3{\cdot}6H_2O$ [1.8 mmol $Ce(NO_3)_3{\cdot}6H_2O$ and 0.2 mmol $Fe(NO_3)_3{\cdot}9H_2O$] were added to 50 mL polyols in a three-neck round-bottomed flask and stirred at 100 °C for 0.5 h. Once a homogeneous, clear solution was obtained, the solution was heated to 180 °C (150 °C for CeO_2-EG: the boiling point of EG is $\approx$197 °C, which is much lower than those of DEG, TEG, and PEG) and kept for 0.5 h. After cooling to

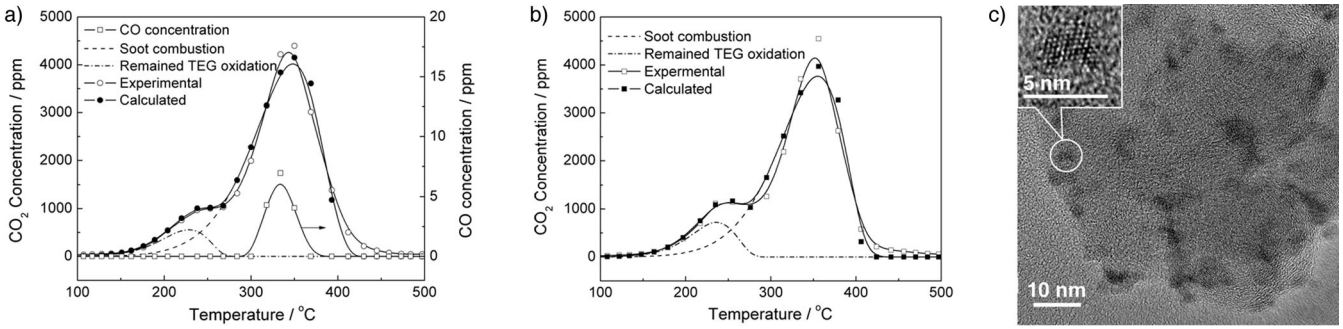

Figure 9. a) Experimental and calculated TPO curves of CeO_2 QDs and soot mixture; b) experimental and calculated TPO curves of Ce–Fe QDs and soot mixture; c) TEM image of the distribution of CeO_2 QDs on soot.

room temperature, the products were washed in toluene to dissolve the un-reacted organic molecules, and the suspension was centrifuged (10000 rpm, 10 min). The washing process was repeated three times. Finally, the solid products were obtained by drying under vacuum at 70 °C for 48 h.

Characterization of materials

X-ray powder diffraction (XRD) patterns were recorded by using a Rigaku D/max-2500 PC diffractometer employing $Cu_{K\alpha}$ radiation ($\lambda = 1.5418$ Å) operating at 50 kV and 200 mA. The crystallite size (D) was calculated using Scherrer's formula [Eq. (1)]:

$$D = \frac{K\lambda}{\beta \cos\theta} \quad (1)$$

For which λ is the wavelength of the radiation used ($\lambda =$ 0.15418 nm for $Cu_{K\alpha}$); β is the full width at half maximum of the diffraction peak considered; K is a shape factor, taken to be 1.0; and θ is the diffraction angle at which the peak appears. The instrumental broadening in the pattern of the sample was corrected using a standard quartz sample.[36]

The UV/vis absorption spectra were recorded by using a Shimadzu UV-2450 spectrophotometer using a quartz cell (1 cm path length). The optical absorption coefficient α was calculated according to Equations (2) and (3):

$$\alpha = (2.303 * 10^3 A\rho)/lc \quad (2)$$

For which A is the absorbance of a sample, ρ is the real density of CeO_2 (7.28 g cm^{-3}), l is the path length, and c is the concentration of the ceria solutions.

$$\alpha \infty \frac{\sqrt{hv - E_d}}{hv} \quad (3)$$

For which E_d is the band gap energy for direct transitions and hv is the photon energy. From the intersection of the extrapolated linear portion, the E_d values of the CeO_2 QDs can be determined. High-resolution transmission electron microscopy (HRTEM) equipped with energy dispersive spectroscopy (EDS) was conducted by using a JEOL JEM-2010 at an accelerating voltage of 200 kV. The particle size distribution histogram was measured with dynamic light scattering (DLS) using a Zetasizer Nano ZS instrument. Field emission scanning electron microscopy (FESEM) equipped with EDS was conducted by using a Hitachi SU-70. Fourier transform infrared (FTIR) spectra were recorded in the range of 370–4000 cm^{-1} using a BRUKER Tensor 27 spectrometer under ambient conditions. ^{1}H NMR spectra were recorded in D_2O by using a Bruker Advance III 400 MHz spectrometer. The Brunauer–Emmett–Teller (BET) surface areas were measured by N_2 adsorption/desorption using a Micromeritics 2020 M instrument. Before N_2 physisorption, the sample was outgassed at 70 °C for 5 h.

Thermogravimetry/Differential Thermal Analysis (TG/DTA) of $Ce(NO_3)_3{\cdot}6H_2O$ was carried out using a PerkinElmer Diamond apparatus with a heating rate of 10 °C min^{-1} in a flowing N_2 atmosphere from room temperature to 900 °C.

Catalytic reactions

The temperature-programmed oxidation (TPO) reactions were conducted in a fixed bed micro reactor consisting of a quartz tube (6 mm i.d.). Printex-U from Degussa was used as the model soot. The FBCs were supported on soot with a weight ratio of 9:1 by a deposition/precipitation method. After drying in vacuum, the mixture of soot and FBCs was milled below 48 μm. A 50 mg sample, diluted with silica to aid heat transfer, is pretreated at 200 °C for 30 min in high purity He (30 mL min^{-1}), and then heated from room temperature to 500 °C at a heating rate of 5 °C min^{-1} in a flow of 10 vol.% O_2+He at a flow rate of 100 mL min^{-1}. The outlet concentrations in the product gas were measured online by a gas chromatograph (SP-6890, Shandong Lunan Ruihong Chemical Instrument Corporation, China) fitted with a methanator. A flame ionization detector (FID) was employed to determine CO and CO_2 concentrations after separating these gases over a Porapak Q column and converting them into methane over a Ni catalyst at 360 °C. The activity for soot combustion is evaluated by the value of T_{max}, which is defined as the temperature at which the rate of soot combustion reaches a maximum.[2] The selectivity to CO_2 formation is defined as the percentage CO_2 outlet concentration divided by the sum of the CO_2 and CO outlet concentrations.

Acknowledgements

This work was supported by the 863 program of the Ministry of Science and Technology of the People's Republic of China (No. 2008AA06Z320), the National Natural Science Foundation of China (No. 21077043 and 21007019) and State Key Laboratory of Environmental Chemistry and Ecotoxicology, Research Center for Eco-Environmental Sciences, Chinese Academy of Sciences (KF2009-13).

Keywords: cerium · fuel-borne catalyst · hydrolysis · polyol · quantum dots

[1] B. A. A. L. van Setten, M. Makkee, J. A. Moulijn, *Catal. Rev.* **2001**, *43*, 489–564.
[2] Z. L. Zhang, Y. X. Zhang, Z. P. Wang, X. Y. Gao, *J. Catal.* **2010**, *271*, 12–21.
[3] Z. L. Zhang, Y. X. Zhang, Q. Y. Su, Z. P. Wang, Q. Li, X. Y. Gao, *Environ. Sci. Technol.* **2010**, *44*, 8254–8258.
[4] S. Biamino, P. Fino, D. Fino, N. Russo, C. Badini, *Appl. Catal. B* **2005**, *61*, 297–305.
[5] J. F. Xu, J. Liu, Z. Zhao, J. X. Zheng, G. Z. Zhang, A. J. Duan, G. Y. Jiang, *Catal. Today* **2010**, *153*, 136–142.
[6] H. M. An, P. J. McGinn, *Appl. Catal. B* **2006**, *62*, 46–56.
[7] T. Campenon, P. Wouters, G. Blanchard, P. Macaudiere, *SAE Tech. Paper*, p. **2004**-01-0071.
[8] J. Kašpar, P. Fornasiero, M. Graziani, *Catal. Today* **1999**, *50*, 285–298.
[9] A. Trovarelli in *Catalysis by Ceria and Related Materials*, Imperical College Press, London, **2002**.
[10] V. Harlé, C. Pitois, L. Rocher, F. Garcia, *SAE Tech. Paper*, p. 2008-01-0331.
[11] Z. L. Zhang, D. Han, S. J. Wei, Y. X. Zhang, *J. Catal.* **2010**, *276*, 16–23.
[12] N. Uekawa, M. Ueta, Y. J. Wu, K. Kakegawa, *Chem. Lett.* **2002**, 854–855.
[13] E. Muccillo, R. Rocha, S. Todokoro, J. Rey, R. Muccillo, M. Steil, *J. Electroceram.* **2004**, *13*, 609–612.
[14] R. D. Purohit, B. P. Sharma, K. T. Pillai, A. K. Tyagi, *Mater. Res. Bull.* **2001**, *36*, 2711–2721.
[15] M. Inoue, M. Kimura, T. Inui, *Chem. Commun.* **1999**, 957–958.
[16] J. X. Xu, G. S. Li, L. P. Li, *Mater. Res. Bull.* **2008**, *43*, 990–995.
[17] K. Nakagawa, Y. Murata, M. Kishida, M. Adachi, M. Hiro, K. Susa, *Mater. Chem. Phys.* **2007**, *104*, 30–39.
[18] S. Phoka, P. Laokul, E. Swatsitang, V. Promarak, S. Seraphin, S. Maensiri, *Mater. Chem. Phys.* **2009**, *115*, 423–428.
[19] T. Masui, K. Fujiwara, K. Machida, G. Adachi, T. Sakata, H. Mori, *Chem. Mater.* **1997**, *9*, 2197–2204.
[20] J. S. Lee, S. C. Choi, *Mater. Lett.* **2005**, *59*, 395–398.
[21] M. Zawadzki, *J. Alloys Compd.* **2008**, *454*, 347–351.

[22] R. X. Valenzuela, G. Bueno, A. Solbes, F. Sapiña, E. Martínez, V. Cortés Corberán, *Top. Catal.* **2001**, *15*, 181 – 188.
[23] W. Cai, J. Q. Wan, *J. Colloid Interface Sci.* **2007**, *305*, 366 – 370.
[24] C. Feldmann, *Scripta Mater.* **2001**, *44*, 2193 – 2196.
[25] C. Feldmann, *Adv. Funct. Mater.* **2003**, *13*, 101 – 107.
[26] C. Feldmann, *Adv. Mater.* **2001**, *13*, 1301 – 1303.
[27] J. Merikhi, H. Jungk, C. Feldmann, *J. Mater. Chem.* **2000**, *10*, 1311 – 1314.
[28] B. Liu, B. B. Liu, Q. J. Li, Z. P. Li, R. Liu, X. Zou, W. Wu, W. Cui, Z. D. Liu, D. M. Li, B. Zou, T. Cui, G. T. Zou, *J. Alloys Compd.* **2010**, *503*, 519 – 524.
[29] C. Ho, J. C. Yu, T. Kwong, A. C. Mak, S. Lai, *Chem. Mater.* **2005**, *17*, 4514 – 4522.
[30] X. S. Tang, E. S. G. Choo, L. Li, J. Ding, J. M. Xue, *Langmuir* **2009**, *25*, 5271 – 5275.
[31] D. Caruntu, G. Caruntu, Y. X. Chen, C. J. O'Connor, G. Goloverda, V. L. Kolesnichenko, *Chem. Mater.* **2004**, *16*, 5527 – 5534.
[32] J. Yang, C. X. Li, Z. W. Quan, D. Y. Kong, X. M. Zhang, P. P. Yang, J. Lin, *Cryst. Growth Des.* **2008**, *8*, 695 – 699.
[33] D. B. Yu, S. H. Yu, S. Y. Zhang, J. Zuo, D. B. Wang, Y. T. Qian, *Adv. Funct. Mater.* **2003**, *13*, 497 – 501.
[34] F. A. Carey in *Organic Chemistry, McGraw-Hill*, New York, **1987**.
[35] Z. L. Zhang, Y. X. Zhang, Z. G. Mu, P. F. Yu, X. Z. Ni, S. L. Wang, L. S. Zheng, *Appl. Catal. B* **2007**, *76*, 335 – 347.
[36] A. Kumar, S. Babu, A. S. Karakoti, A. Schulte, S. Seal, *Langmuir* **2009**, *25*, 10998 – 11007.

Received: May 30, 2011
Published online on August 29, 2011

